

Journal of Materials Chemistry A

Accepted Manuscript



This is an *Accepted Manuscript*, which has been through the Royal Society of Chemistry peer review process and has been accepted for publication.

Accepted Manuscripts are published online shortly after acceptance, before technical editing, formatting and proof reading. Using this free service, authors can make their results available to the community, in citable form, before we publish the edited article. We will replace this *Accepted Manuscript* with the edited and formatted *Advance Article* as soon as it is available.

You can find more information about *Accepted Manuscripts* in the [Information for Authors](#).

Please note that technical editing may introduce minor changes to the text and/or graphics, which may alter content. The journal's standard [Terms & Conditions](#) and the [Ethical guidelines](#) still apply. In no event shall the Royal Society of Chemistry be held responsible for any errors or omissions in this *Accepted Manuscript* or any consequences arising from the use of any information it contains.



Journal Name

ARTICLE

One-step, template-free synthesis of highly porous nitrogen/sulfur-codoped carbons from a single protic salt and their application to CO₂ capture

Received 00th January 20xx,
Accepted 00th January 20xx

DOI: 10.1039/x0xx00000x

www.rsc.org/

Shiguo Zhang, Zhe Li, Kazuhide Ueno, Ryoichi Tatara, Kaoru Dokko and Masayoshi Watanabe*

Traditional methods of preparing highly porous, nitrogen/sulfur-codoped carbons require either template-based tedious, time-consuming procedures or harsh chemical/physical activation process. In this paper, we report a very facile method to prepare such carbons via the direct carbonization of a single protic salt, prop-2-en-1-aminium hydrogensulfate, in the absence of any hard/soft template or activation agent. Depending on the carbonization temperatures, the obtained carbons exhibited tunable structures and properties, in terms of their morphologies, surface areas, pore structures, and chemical compositions. Particularly, the carbon material obtained at 1000 °C showed a very large surface area (1149 m²/g), even comparable to that of traditionally activated carbon. Among all the samples, the carbon obtained at 900 °C, exclusively having a narrowly distributed microporous structure, exhibited a significant CO₂ uptake of 2.58 mmol/g at 298 K and 1 atm. This carbon could also be easily regenerated and reused without any evident loss of CO₂-adsorption capacity.

Introduction

Porous carbon materials have many potential applications in diverse areas, including chemical catalysis, fuel cells, lithium batteries, supercapacitors, and adsorption materials owing to their attractive features of low costs, large surface areas, light weights, good processabilities, high chemical and thermal stabilities, high electronic conductivities, and controllable heteroatom-doping potentials. Considering their importance in practical applications, many efforts have been devoted to developing novel organic precursors and tailoring the structures and properties of porous carbons by various procedures. Because most organic compounds are either completely evaporated or decomposed into gaseous products during high-temperature carbonization, the current precursors available are therefore rather limited to natural or synthetic polymers with low vapor pressures such as polyacrylonitrile,¹ phenolic resins,^{2,3} and other biomass.⁴ In order to address the issues of limited solubility and complicated syntheses associated with polymer precursors, a series of novel precursors, such as ionic liquids,⁵⁻⁹ metal-organic frameworks (MOFs),¹⁰⁻¹³ and zeolite-imidazolate frameworks (ZIFs),^{14, 15} have recently been explored as potential precursors. Doping heteroatoms such as nitrogen and sulfur into the carbon hexagonal rings has reportedly imparted improved oxidative stability,¹⁶ catalytic activity,¹⁷⁻²⁰ and basicity²¹ to the carbon materials under study. The obtained

heteroatom-doped, porous carbons have been intensively explored as either electrocatalysts and/or electrode materials for energy storage and conversion. Generally, heteroatom-doped carbons, for example, N-doped, porous carbons can be synthesized by the following two methods, namely, *in situ* carbonization from N-containing precursors, such as polypyrrole,²² polydopamine,²³ polyaniline,²⁴ and polyamides,²⁵ or post-treatment of as-obtained carbons with N-containing agents such as NH₃ and CH₃CN.²⁶ The former method is highly desirable not only because it can simplify the entire process but also because it allows a homogeneous distribution of N atoms throughout the carbon material.¹⁷ In contrast, the complicated post-treatment may result in morphological defects and structural degradation of the carbon materials, including collapse and blockage of the porous architecture.²⁷

In addition, it is well known that highly porous carbons (surface area > 1000 m²/g) are generally obtained via the templating carbonization of organic precursors^{28, 29} or physical (CO₂)^{30, 31} or chemical (KOH³²⁻³⁴ or ZnCl₂³⁵) activation of the as-synthesized carbons. These methods, however, usually require additional, tedious, time-consuming procedures, involving the synthesis of both precursors and templates, infiltration of precursors into the template, carbonization, and template-removal via etching or a harsh activation process. Compared to the complicated templating and activation methods, a one-step, template-free synthesis of porous carbons via the direct carbonization of organic precursors is highly attractive and more feasible overall.^{6, 36-41} Because in such case the precursors have to serve an "all-in-one" role, including acting as both carbon source and self-template with high thermal stability, there have only been a few reports on the direct synthesis of porous carbons to date. Generally, these reports have focused on

* Department of Chemistry and Biotechnology, Yokohama National University, 79-5 Tokiwadai, Hodogaya-ku, Yokohama 240-8501, Japan.

† Footnotes relating to the title and/or authors should appear here. Electronic Supplementary Information (ESI) available: [details of any supplementary information available should be included here]. See DOI: 10.1039/x0xx00000x

the direct carbonization of specific nitrile-containing ionic liquids,⁴² microphase-separated block copolymers,⁴³ MOFs,¹⁰⁻¹³ ZIFs,^{14,15} and metal-containing salts.⁴⁴⁻⁴⁷ Ionic liquids and block polymers are expensive and difficult to synthesize, while for metal-containing precursors (MOFs, ZIFs, and metal-containing salts), an additional etching step is required to remove the metal impurities. Moreover, the absence of N heteroatoms and the less developed porous structures in most of the obtained carbons strongly hinder their applications.

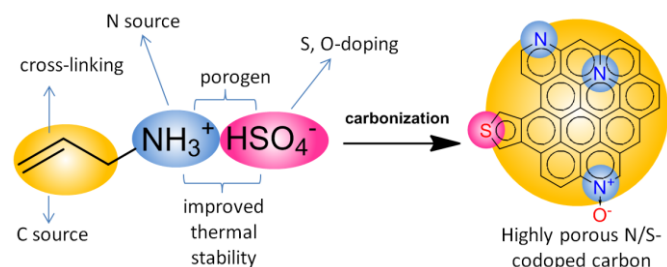


Figure 1. One-step template-free synthesis of highly porous, N/S-codoped carbons from a single protic salt ([Allyl-NH₃][HSO₄]).

Meanwhile, selective capture and storage of CO₂ has recently attracted considerable attention because CO₂ is a major greenhouse gas and a renewable carbon source. Many different types of CO₂-sorbing, porous materials such as amine-functionalized, mesoporous silicas,⁴⁸ MOFs,⁴⁹ nanoporous organic polymers,⁵⁰ and porous carbons,⁵¹ have been explored. Among them, N-doped porous carbons have proven to be one of the most promising set of candidates for CO₂ capture, storage, and separation⁵²⁻⁵⁷ for the following reasons. First, carbon materials can be easily obtained in large quantities. Second, porous carbon materials, due to their low densities, generally exhibit larger surface areas and pore volumes per unit mass than do MOFs and silicas. Third, unlike porous silicas and MOFs that often suffer from low chemical stabilities especially under hydrolytic conditions, carbon materials are chemically inert and robust under various conditions. More importantly, relatively strong interaction between the acidic CO₂ molecules and the basic N sites on pore walls may account for their great potentials for physisorption and for the regeneration of CO₂.⁵²

Herein, we report a very facile method to prepare highly porous N/S-codoped carbons via a direct, template-free carbonization of a single, easily prepared, low-cost protic salt, prop-2-en-1-aminium hydrogensulfate ([Allyl-NH₃][HSO₄]) (Figure 1). The carbonization, N doping, and pore formation were achieved through one-step pyrolysis without purification, post-treatment, or an activation process. The entire process was very simple and easy to implement. Some of the N-doped carbons that had large surface areas or narrowly distributed micropores exhibited significant CO₂-adsorption capacities.

Experimental Materials and Methods

Materials Synthesis. [Allyl-NH₃][HSO₄] was synthesized according to the established procedure.^{8,53} The obtained protic salt was subjected to direct carbonization in a tube furnace under an Ar atmosphere (100 mL/min) using the following temperature program: (1) degassing at room temperature for 1 h; (2) heating to 250 °C at a rate of 10 °C/min; (3) further heating to 350 °C at a rate of 2 °C/min; (4) heating to the desired temperature (e.g., 1000 °C) at a rate of 10 °C/min; and finally, (5) maintaining the sample at this temperature for 2 h. After cooling the sample to room temperature, the obtained carbon materials were powdered for further characterization.

Characterization. Thermogravimetric analysis (TGA) was performed using a thermogravimetry/differential thermal analyzer (TG-DTA 6200, Seiko Instruments). The temperature was increased from room temperature to 1000 °C under an Argon flow of 100 mL min⁻¹ with open alumina pans. Powder X-ray diffraction (XRD) patterns were collected on a Rigaku RINT-2000 diffractometer using Cu K α ($\lambda = 0.154$ nm) radiation. The diffractograms were recorded in the 2 θ range from 10° to 90° with a 2 θ step size of 0.02 and a scanning speed of 10°/min. Chemical states, compositions, and valence-band spectra were analyzed by a PHI Quantera SXM X-ray photoelectron spectrometer (XPS) with a base pressure of 6.7 $\times 10^{-8}$ Pa with an Al K α (1486.6 eV) X-ray source, and a pass energy of 280.00 (survey scan) or 69.00 eV (high-resolution scan). Nitrogen-sorption isotherms were recorded on a Belsorp-Mini II sorption analyzer (BEL Japan, Inc.) at -196 °C (77 K). Prior to the measurements, the samples were purged with flowing nitrogen at 300 °C for 3 h. The specific surface areas (S_{BET}) were calculated using the Brunauer–Emmett–Teller (BET) method at relative pressures (p/p_0) of 0.01–0.2. The total pore volumes (V_{tot}) were determined from the amounts of N₂ uptake at p/p_0 of 0.99. CO₂-adsorption experiments were recorded on a Belsorp-Mini II sorption analyzer at 0 °C and 25 °C. The cumulative surface areas, cumulative pore volumes, and pore-size distributions were calculated using the non-local density-functional-theory (NLDFT) method (slit/cylinder pores). Raman spectra were measured using a 532-nm laser Raman spectrometer RMP-300 (JASCO, Japan) at room temperature. The surface morphologies and composition analyses were conducted on a field-emission scanning electron microscope (JSM-7001F, JEOL Ltd.) with an energy dispersive spectroscopy (EDS) accessory (EDAX, USA). Elemental analysis for carbon, nitrogen, sulfur, and hydrogen was performed with a Vario-EL III CHNS elemental analyzer.

Results and Discussion

[Allyl-NH₃][HSO₄] was synthesized via a simple neutralization, followed by solvent removal. The obtained protic salt was subjected to direct carbonization at temperatures of 700, 800, 900, and 1000 °C. The resultant carbon materials were denoted as AN-7, AN-8, AN-9, and AN-10, respectively. It

should be noted that the entire process was conducted without pretreatment, post-treatment, or any activation steps. Based on the established correlations between precursors and carbons,⁵³ the protonation likely improved the thermal stability of allylamine for successful carbonization, while the allyl group served as both a carbon source and a cross-linking moiety simultaneously. In addition, the amine behaved as a nitrogen source, while sulfur and oxygen might have been partially codoped into the final carbon materials (Figure 1). In order to throw light on the variation of carbon with calcination temperature, the TGA of [Allyl-NH₃][HSO₄] was measured and shown in Figure S1. The weight loss for the first stage observed at 170–280 °C is ca. 61%, which is very close to the weight percent of anion in the precursor. The second-stage weight loss observed at 280–470 °C is ca. 14%, which is very close to the combined weight percent of N and H in the precursor. Even though the detailed carbonization mechanism is still not clear at present because carbonization is a complicated process wherein multiple chemical reactions occur simultaneously, the above TG result possibly suggested that most of the anions were removed during the first decomposition stage, while the formation of polycyclic aromatic compounds via cross-linking polymerization, deamination and dehydrogenation may account for the second stage. The slight but continuous weight loss above 500 °C could be due to the further transformation into carbon materials via denitrogenation, desulfuration, deoxygenation, and dehydrogenation.

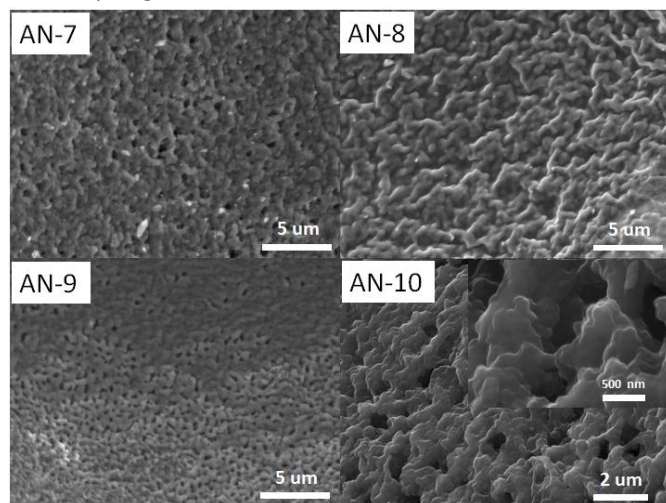


Figure 2. FESEM images of carbons derived from [Allyl-NH₃][HSO₄].

The morphologies of the samples obtained at different temperatures were investigated via field-emission scanning electron microscopy (FESEM), as shown in **Figure 2**. AN-7 consisted of large numbers of micrometer-sized block particles with irregular shapes that seemed to be randomly agglomerated into large species and resulted in the amorphous nature with macroscopic cavities or holes in between the formed block nanoparticles. As the temperature increased to 800 °C, the carbon particles were partially fused into bulk architectures. As the temperature further increased to 900 °C, the as-synthesized carbon product AN-9 was highly

porous with the presence of more homogeneously distributed, disordered pores. Meanwhile, the sizes of the macropores decreased from the micrometer scale to around 500 nm. For AN-10, obtained at 1000 °C, the FESEM image shows a microstructure with numerous interconnected macropores. The inset in Figure 2 presents a higher-magnification image, which reveals a closely layered yet distorted microstructure, indicating the formation of a continuous three-dimensional pore network. Taking into account the self-templating carbonization/decomposition of [Allyl-NH₃][HSO₄] at elevated temperatures, nanoscale porous structures likely formed within the carbon products and should be detectable via the following N₂ adsorption/desorption analysis. More importantly, the unique open-pore system at the surface would provide a short diffusion path for gas molecules.

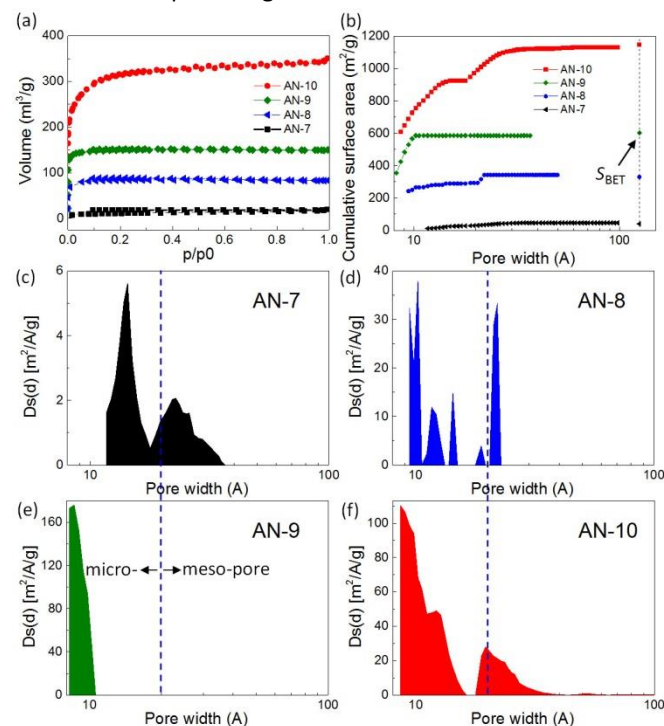


Figure 3. N₂ sorption isotherms (for enlarged scale at p/p_0 of 0–0.1, see **Figure S2**), distribution of cumulative surface area, and pore-size distribution of [Allyl-NH₃][HSO₄]-derived carbons. The blue, broken lines indicate the border between micropore and mesopore structures.

Table 1. Specific surface area (S_{BET} , m²/g), pore volume (V_{tot} , cm³/g), surface elemental composition (at%, determined by XPS), and CO₂-uptake capacity (mmol/g) measured at 298 K for [Allyl-NH₃][HSO₄]-derived carbon materials.

Carbon	S_{BET}	V_{tot}	C	N	S	O	CO ₂
AN-10	1149	0.540	88.3	2.7	1.2	7.8	2.40
AN-9	603	0.232	90.6	2.6	1.7	5.1	2.58
AN-8	330	0.128	90.3	3.0	1.0	5.6	2.31
AN-7	40	0.031	86.7	6.0	1.8	5.5	2.08

In order to explore the pore structure of the [Allyl-NH₃][HSO₄]-derived carbons, the nitrogen-adsorption and

desorption isotherms were recorded. As shown in **Figure 3(a)**, nearly all of the carbons displayed a Type-I curve with significant capillary condensation at low relative pressures ($P/P_0 < 0.1$) according to the IUPAC classification⁵⁸ without any obvious hysteresis loop, indicating the presence of a large number of micropores in AN-X. The specific surface areas (S_{BET}) and pore volumes (V_{tot}) calculated using the Brunauer–Emmett–Teller (BET) method are summarized in **Table 1**. Interestingly, as the carbonization temperature increased from 700 °C to 1000 °C, the surface area of AN-X was remarkably enhanced from 40 m²/g to 1149 m²/g, and the V_{tot} was increased from 0.031 cm³/g to 0.540 cm³/g. Considering that the entire process to prepare AN-X involved only neutralization and carbonization, the large S_{BET} for AN-10 obtained via such a simple method is of great significance. The very large surface area obtained in the absence of both hard and soft templates was related to the unique structure of the protic salt. Pyrolysis of the protic salt likely occurred via the involvement of the primary aliphatic-amine group.⁵⁹ The major part of the N-containing base and the anion were sacrificed as a porogen or self-template to generate large amounts of pores.⁵³ Notably, AN-10 had a surface area much larger than those of most other directly carbonized porous carbons from large-surface-area, microporous, imine-linked polymers (344 m²/g),³⁶ nitrile-containing ionic liquids (780 m²/g),⁶ or self-assembled block copolymers (500 m²/g),³⁹ and were even comparable to N-doped, microporous carbons derived from an MOF (1172 m²/g)³⁷ or activated carbons using CO₂ (1140 m²/g)³⁹ or harsh KOH (1260 m²/g).³² The cumulative surface area as a function of the pore size was further analyzed using the NLDFT method (slit/cylinder pores). **Figure 3(b)** reveals that the cumulative surface areas for all the carbons obtained with 4.0-nm-pore-sizes corresponded very well with the S_{BET} calculated by the BET method. More specifically, the cumulative surface areas for both AN-8 and AN-10 were saturated at 3.5 nm, while AN-7 attained the highest value at 2.2 nm. Very interestingly, nearly the entire surface area of AN-9 was covered by pores smaller than 1.0 nm. In contrast, the very large surface area of AN-10 was ascribed to the co-contribution of two types of pores, that is, micropores (<1.5 nm) and small mesopores (1.8–3.0 nm). The result of the pore-size distributions (PSDs) shown in **Figures 3(c)–3(f)** further confirmed the conclusion drawn from the distribution of the cumulative surface areas. The very noticeable result is that AN-9 was exclusively microporous with a very narrow PSD centered at 0.86 nm; this highly microporous structure should be beneficial for CO₂ capture, as discussed below.

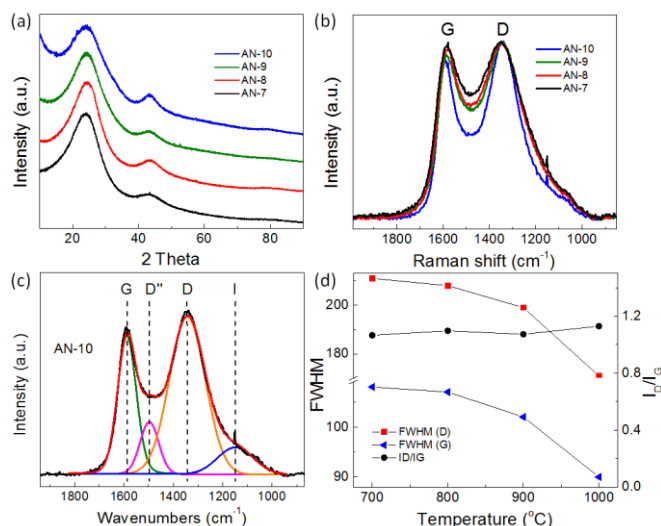


Figure 4. (a) XRD patterns and (b) Raman spectra of [Allyl-NH₃][HSO₄]-derived carbons. (c) Deconvolution of the Raman spectrum of AN-10. (d) The $I_{\text{D}}/I_{\text{G}}$ ratios and FWHMs of the G and D bands as functions of the carbonization temperatures.

The graphitization behavior of the carbons derived from [Allyl-NH₃][HSO₄] was investigated via XRD patterns and Raman spectra. As shown in **Figure 4(a)**, the XRD pattern of AN-7 showed a (002) diffraction peak centered at $2\theta = 24.0^\circ$ and a clearly observable (100) reflection characteristic at $2\theta = 43.3^\circ$, indicating that AN-7 had a partially graphitic structure. With increasing pyrolysis temperature, although no obvious shift of the peak position for either (002) or (100) was observed, the peak representing (100) diffraction became more pronounced, implying an improved degree of graphitic nature at higher temperatures. **Figure 4(b)** depicts the Raman spectra of the carbons obtained at different pyrolysis temperatures. Clearly, they showed two broad peaks that could be approximately assigned to the G and D bands at 1346 and 1583 cm⁻¹, respectively, similar to the observed results in most N-doped carbons and highly N-doped nanotubes.^{46, 60–62} The G mode had E_{2g} symmetry that involved the in-plane bond-stretching motions of pairs of sp²-hybridized C atoms, and this mode does not require the presence of a six-membered ring. Thus, it occurred at all sp² sites, not only those in rings. In contrast, the D peak was a breathing mode with A_{1g} symmetry involving phonons near the K zone boundary. This mode is forbidden in perfect graphite and only becomes active in the presence of defects such as edges, functional groups, or structural disorders.^{63, 64} It is expected that any distortion in the pure-carbon hexagonal lattice, for example, in the case of heteroatom doping, will result in an increase in the D-band intensity.⁶⁵ In most reports on carbons, only the $I_{\text{D}}/I_{\text{G}}$ ratios have been arbitrarily used to investigate the graphitic structures. In fact, in addition to the $I_{\text{D}}/I_{\text{G}}$, both the band positions and the full width at half maximum (FWHM) of the Raman bands are reported to be strongly related to the defects and the disorder structure in carbons.^{63, 66}

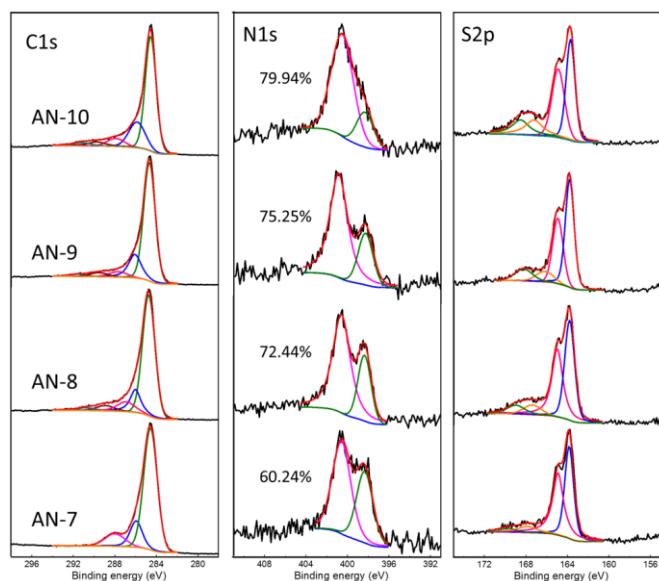


Figure 5. High resolution C 1s, N 1s, and S 2p XPS spectra of [Allyl-NH₃][HSO₄]-derived carbons. Numbers in the N 1s spectra indicates the percentage of graphitic N.

As for these carbons derived from [Allyl-NH₃][HSO₄], all the Raman spectra were comparable in terms of the peak positions, while an attempt to simply deconvolute them into just two Lorentzian or Gaussian shapes failed. Therefore, the raw spectra were fitted to four bands, denoted as G, D, G', and I [Figure 4(c) and Figure S3], according to standard conventions.^{60, 67, 68} The results shown in Figure 4(d) revealed that there were no obvious correlations between I_D/I_G and the carbonization temperatures, and the I_D/I_G values for all the carbons were in the narrow range of 1.023 to 1.114. However, the carbons obtained at higher temperatures clearly showed much narrower G and D bands. For example, the FWHM of the G band was greatly decreased from 108 cm⁻¹ for AN-7 to 90 cm⁻¹ for AN-10, while the corresponding FWHM for the D band decreased from 211 to 171 cm⁻¹ [Figure 4(d)]. These results confirmed that the high carbonization temperature likely yielded a more graphitic structure, as expected. It should be noted that the heteroatoms, which imparted structural irregularity to the hexagonal rings in the graphene layers, might have released at high temperatures, alleviating the number of defects and improving the graphitization.

As functions of an evolution of the temperature, the surface states of the carbons were investigated via XPS. The results are depicted in Figure 5 and summarized in Table 1. The survey spectra revealed the presence of carbon, nitrogen, oxygen, and sulfur in all the carbon materials without any other impurities and wherein the O signal was presumed to be from either the anions or adsorbed air or water. All of the obtained carbons contained mainly C (86-91 at%), suggesting that the major part of the protic salt, that is, -NH₃⁺, and HSO₄⁻, was completely decomposed into volatile gaseous molecules, as expected. For AN-7, the C 1s spectrum could be resolved into three components: the main component at 284.6 eV corresponded to the graphene-like sp²-bonded carbons of the aromatic structures,⁶⁹ while the second one at 28.0 eV with a

lower intensity was attributed to the carbon bonded to N, S, or O species. The third small peak could be ascribed to the formation of functional groups such as C=O. As the temperature increased to 800 °C, the intensity of the peak at 286.0 eV decreased, while several weak but distinct π-π* shake-up peaks were observed on the high-energy side. These satellites are frequently observed in atoms involved in multiple bonds and are characteristic of delocalized systems with multiple bonding, aromatic compounds and conjugated carbon materials.⁷⁰ In contrast, the N 1s spectra for all the carbons were dominated by two N species, i.e., pyridinic N (398.3 eV) and graphitic-type quaternary N structures (400.6 eV), which are typically observed for N-doped carbons.^{71, 72} The percentage of the quaternary N component first greatly increased from 60.24% for AN-7 to 72.44% for AN-8 and then slightly increased to 79.94% for AN-10. Meanwhile, the total N content was first significantly reduced from 6.0 at% for AN-7 to 3.0 at% for AN-8 and then became stable (2.6-3.0 at%). The decrease in the total N content as well as the percentage of pyridinic N atoms at higher temperatures is a common feature of N-doped carbons⁷²⁻⁷⁴ because the graphitic N atoms are much more stable than pyridinic N atoms at high temperatures. Therefore, the thermally unstable pyridinic N atoms were continuously released during heating. Meanwhile, condensation from pyridinic N atoms to valley and central graphitic N atoms occurred.⁷³ The evolution of the N 1s as well as the C 1s signals for all of the [Allyl-NH₃][HSO₄]-derived carbons implied the increased degree of condensation and conjugation within the carbonaceous structures with increasing carbonization temperature from 700 °C to 800 °C. The S 2p signals (<2.0 at%) in all the carbons could be resolved into four well-defined peaks at binding energies of approximately 163.8, 164.9, 167.9, and 169.7 eV. The former two peaks corresponded to the S 2p_{3/2} and S 2p_{1/2} of the sulfide groups (-C-S-C-), while those of the higher binding energies were ascribed to oxidized species (-C-SO_x-C-, x = 2-4), such as in the form of sulfate or sulfonate.⁷⁵

The EDS analysis further confirmed that the obtained materials were metal-free; only C, N, O, and S were detected (Figure S4). In addition, the EDS elemental-mapping images of AN-9 in Figure 6 indicated a uniform dispersion of these elements in the carbon material, verifying that the in situ direct carbonization of single protic salt provided a facile method to obtain N/S-codoped carbon materials with homogeneous distributions of heteroatoms.

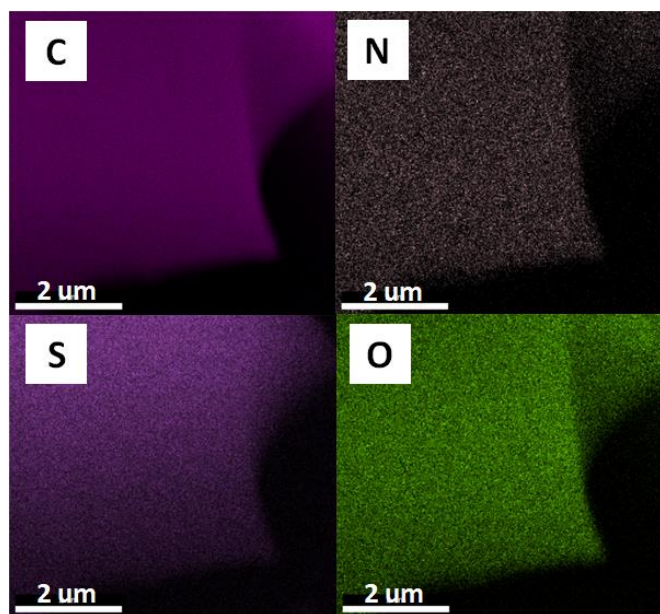


Figure 6. EDS-mapping images of AN-9.

N-doped porous carbons have been reported to be notable sorbents for efficient CO₂ capture.⁵⁴⁻⁵⁷ The N-containing groups in porous carbons can act as Lewis-base sites, efficiently binding acidic CO₂ molecules via an acid-base interaction. CO₂-adsorption capacities for all carbons derived from [Allyl-NH₃][HSO₄] were measured at 0 °C and 25 °C. As shown in Figure 7, the shapes of the adsorption isotherms were typical for solid adsorbents with a relatively rapid rise in adsorption at low pressures, followed by a more linear rise at higher pressures.⁷⁶ More specifically, the adsorption isotherms at low pressures (< 0.1 atm) increase more steeply for AN-X obtained at lower temperatures such as AN-7 and AN-8, especially at 0 °C. In combination with the XPS analysis, these distinct results could be ascribed to the fact that the total N content as well as the percentage of the more basic N species (pyridinic N) decreased with the increasing carbonization temperature from 700 to 1000 °C. At 0 °C and 1 atm, the adsorption capacities increased monotonously with increasing carbonization temperature [Figure 7(a)], ranging from 2.67 mmol/g (AN-7) to 3.77 mmol/g (AN-10). These results indicated that at low pressures uptake might have correlated with the interaction between CO₂ molecules and sorbents and that at higher pressures, it correlated with the surface area, the pore volume, and/or the specific pore structure. For example, the lowest capacity observed for AN-7 undoubtedly resulted from its very low surface area (40 m²/g) despite the relatively high N content (total) and high percentage of pyridinic N, and vice versa, AN-10 with the largest surface area had the highest capacity (Table 1).

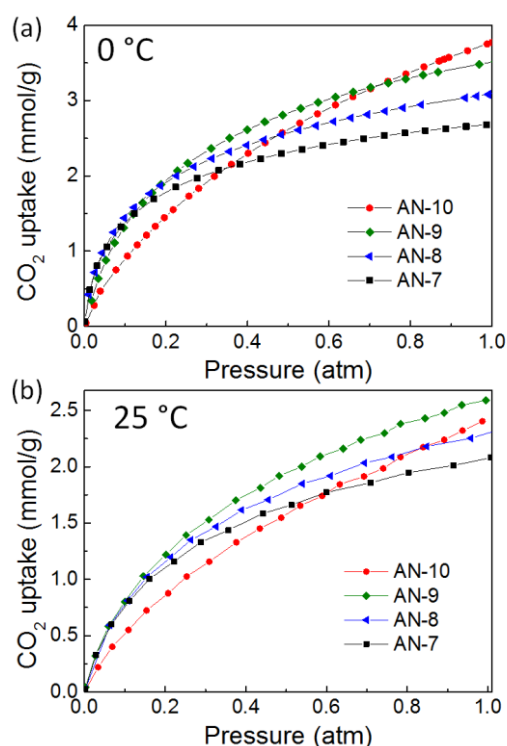


Figure 7. CO₂-adsorption/desorption curves of [Allyl-NH₃][HSO₄]-derived carbons at 0 °C and 25 °C.

The CO₂-adsorption capacity decreased at high temperatures, a common property of porous carbons.⁵² The results of the capacities measured at 25 °C are shown in Table 1. Interestingly, instead of AN-10, AN-9 exhibited the highest CO₂ capacity (2.58 mmol/g) at 25 °C and 1 atm. The significantly higher capacity of AN-9 than that of AN-10 could be because the low content of pyridinic N and thus the lower basicity of AN-10 could not ensure high CO₂-uptake at relatively high temperatures. More importantly, in highly microporous AN-9, the nearly monodistributed micropores (<1.0 nm) strongly accounted for its high capacity despite its relatively low surface area (603 m²/g), as compared to that of AN-10. Micropores can play a significant role in gas adsorption. Especially for CO₂, it has been reported that the presence of micropores of sizes around 1 nm is important for efficient adsorption because of the small molecular size of CO₂ molecules (0.209 nm).⁷⁷⁻⁷⁹ In addition, it should be noted that the capacity of AN-9 was greater than that of commercial activated carbon (< 2 mmol/g)⁵¹ and porous N-doped carbonaceous membrane (1.8 mmol/g)⁸⁰ and was comparable to those of the N-doped porous carbons (ca. 2.5 mmol/g);³⁸ the copolymer-templated N-enriched porous nanocarbons (ca. 2.8 mmol/g);³¹ and the N-doped hollow carbon nanospheres (2.67 mmol/g)⁸¹ that require complicated syntheses.

The capacities for all of the isotherms progressively increased with pressure but did not reach saturation at 1 atm, especially at 25 °C, suggesting improved capacities at higher pressures. To show the regeneration capabilities of the carbon sorbents studied, we performed several adsorption cycles for AN-9 at 25 °C. As shown in Figure 8(a), no evident decreases in the CO₂ uptake for the

adsorption isotherms were observed after five cycles, indicating that these materials could be regenerated. In order to obtain a greater understanding of the distinct uptake behavior between these carbon materials obtained at different temperatures and the interaction of CO₂ with the carbon materials, the isosteric heats (Q_{st}) of adsorption for the different carbon materials were further examined by fitting the CO₂-adsorption isotherms measured at two separate temperatures (0 °C and 25 °C), based on the following Clausius–Clapeyron equation [Eq. (1)].^{76, 82, 83}

$$\ln \frac{P_1}{P_2} = Q_{st} \times \frac{T_2 - T_1}{R \times T_1 \times T_2} \quad (1)$$

where T_1 and T_2 represent a Kelvin temperature at which an isotherm is measured, P_1 and P_2 represent a pressure at which the same adsorbed amount is reached at T , and R is the ideal-gas constant (8.314 J·K⁻¹·mol⁻¹).

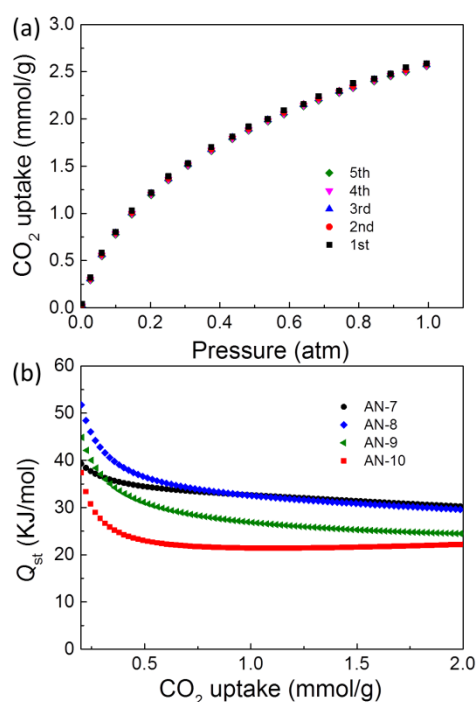


Figure 8. (a) Multicycle CO₂-adsorption isotherms for AN-9 at 25 °C. (b) Isothermic heats of adsorption for [Allyl-NH₃][HSO₄]-derived carbon materials calculated using the Clausius–Clapeyron equation.

The calculated Q_{st} values as a function of the CO₂ uptake for all the carbons are presented in **Figure 8(b)**. The Q_{st} values of the adsorption varied in the range of 37–45 kJ/mol at low-CO₂ uptake values (low surface coverage) and reduced to an average of 20–30 kJ/mol at higher coverage. The Q_{st} values were obviously lower than those expected for chemisorption, as observed for alkylamine-functionalized MOF (90 kJ/mol)⁴⁹ or silicas (100 kJ/mol),⁴⁸ implying that the uptake of CO₂ essentially proceeded via physisorption. However, the Q_{st} values were clearly greater than those reported previously for highly porous activated carbons (19–20 kJ/mol)⁸⁴ or N-doped, high-surface-area, microporous carbons templated from zeolite (16.5–20 kJ/mol),⁸⁵ indicating the strong interaction

between acidic CO₂ molecules and the N-doped-carbon pore walls. More specifically, AN-7, which contained the highest N content and high percentage of pyridinic N and therefore more readily accessible sites for CO₂ adsorption at lower CO₂-uptake values, exhibited the highest Q_{st} value of 30 kJ/mol at higher coverage (2.0 mmol/g) despite its very small surface area, while AN-9 had an intermediate Q_{st} of 24.7 kJ/mol, and AN-10 had the lowest Q_{st} of 22.2 kJ/mol at a CO₂ uptake of 2.0 mmol/g. In combination with the XPS analysis and the CO₂ uptakes at both 0 °C and 25 °C, the N heteroatoms (both N content and percentage of pyridinic N) incorporated into the carbon framework likely played an important role in the initial interaction between CO₂ and the carbon surface and thus the isosteric heats of adsorption, while both N functionality and micropores dominated the CO₂-adsorption capacity at higher pressures. In addition, the relatively high sulfur content in AN-9 (Table 1) may contribute to the high CO₂ uptake, possibly due to the formation of strong pole-pole interactions between the large quadrupole moment of CO₂ molecules and polar sites associated to sulfur functional groups.^{86, 87}

Conclusions

In conclusion, highly porous, N/S-codoped carbons were obtained via the direct, template-free carbonization of a single, low-cost protic salt without additional steps involving prepolymerization, synthesis of a template, post-treatment, or a harsh activation process. N, S, and O were homogeneously distributed in the carbon materials in situ through one-step carbonization. During carbonization, the protic salt likely served as an “all-in-one” precursor, that is, the C source, N and S dopant, and the self-template or porogen. The allyl moiety in the protic salt helped cross-linking polymerization, and the protonation improved the thermal stability of the allylamine for carbonization. On increasing the carbonization temperature from 700 to 1000 °C, the N content decreased from 6.0 at% to 2.7 at%, while the porous structure developed greatly with surface area increasing from 40 m²/g to 1149 m²/g. Further analysis of FESEM images and the pore-size distributions revealed that nearly all of the carbons possessed macropores and micropores simultaneously. The strategy developed here to achieve highly porous, N-doped carbons is more facile compared to traditional templating or activation methods. The economical fabrication process together with the unique pore structures as well as their intrinsic N-doped nature makes these carbons potential sorbents for efficient and reversible CO₂ physisorption. Particularly, AN-9, which possessed a narrowly distributed microporous structure with a surface area mainly covered by pores smaller than 1.0 nm exhibited the highest capacity (2.58 mmol/g at 298 K and 1 atm) for CO₂ adsorption among all the carbon materials studied. This particular carbon is also of essential interest for other applications where small pores are needed. For example, it might have great potential as microporous cathodic host for lithium-sulfur batteries;⁸⁸ these studies are currently underway in our group.

Acknowledgements

This work was supported by the Japan Science and Technology Agency (JST) – Advanced Low Carbon Technology Research and Development Program (ALCA) of Japan.

Notes and references

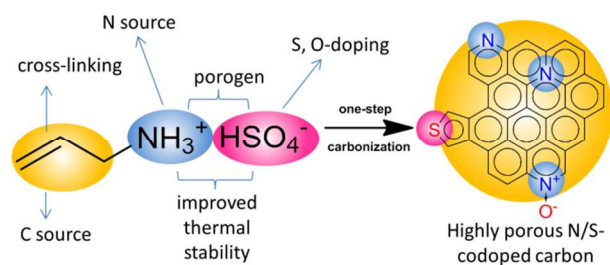
‡ Footnotes relating to the main text should appear here. These might include comments relevant to but not central to the matter under discussion, limited experimental and spectral data, and crystallographic data.

1. T. Kowalewski, N. V. Tsarevsky and K. Matyjaszewski, *J. Am. Chem. Soc.*, 2002, **124**, 10632-10633.
2. C. D. Liang, K. L. Hong, G. A. Guiochon, J. W. Mays and S. Dai, *Angew. Chem. Int. Ed.*, 2004, **43**, 5785-5789.
3. D. Long, J. Zhang, J. Yang, Z. Hu, G. Cheng, X. Liu, R. Zhang, L. Zhan, W. Qiao and L. Ling, *Carbon*, 2008, **48**, 1253-1269.
4. F. Pan, Z. Cao, Q. Zhao, H. Liang and J. Zhang, *J. Power Sources*, 2014, **272**, 8-15.
5. S. Zhang, K. Dokko and M. Watanabe, *Mater. Horiz.*, 2015, **2**, 168-197.
6. J. S. Lee, X. Wang, H. Luo, G. A. Baker and S. Dai, *J. Am. Chem. Soc.*, 2009, **131**, 4596-4597.
7. J. P. Paraknowitsch, J. Zhang, D. Su, A. Thomas and M. Antonietti, *Adv. Mater.*, 2010, **22**, 87-92.
8. S. Zhang, M. S. Miran, A. Ikoma, K. Dokko and M. Watanabe, *J. Am. Chem. Soc.*, 2014, **136**, 1690-1693.
9. S. Zhang, H.-M. Kwon, Z. Li, A. Ikoma, K. Dokko and M. Watanabe, *ChemElectroChem*, DOI: 10.1002/celc.201500129.
10. B. Liu, H. Shioyama, T. Akita and Q. Xu, *J. Am. Chem. Soc.*, 2008, **130**, 5390-5391.
11. J.-W. Jeon, R. Sharma, P. Meduri, B. W. Arey, H. T. Schaefer, J. L. Lutkenhaus, J. P. Lemmon, P. K. Thallapally, M. I. Nandasiri and B. P. McGrail, *ACS Appl. Mater. Inter.*, 2014, **6**, 7214-7222.
12. Y. Hou, T. Huang, Z. Wen, S. Mao, S. Cui and J. Chen, *Adv. Energy Mater.*, 2014, **4**.
13. F. Zheng, Y. Yang and Q. Chen, *Nat. Commun.*, 2014, **5**.
14. P. Zhang, F. Sun, Z. Xiang, Z. Shen, J. Yun and D. Cao, *Energy Environ. Sci.*, 2014, **7**, 442-450.
15. L. Zhang, Z. Su, F. Jiang, L. Yang, J. Qian, Y. Zhou, W. Li and M. Hong, *Nanoscale*, 2014, **6**, 6590-6602.
16. J. P. Paraknowitsch, J. Zhang, D. S. Su, A. Thomas and M. Antonietti, *Adv. Mater.*, 2010, **22**, 87-92.
17. Y. Y. Shao, J. H. Sui, G. P. Yin and Y. Z. Gao, *Appl. Catal. B*, 2008, **79**, 89-99.
18. C. P. Ewels and M. Glerup, *J. Nanosci. Nanotechnol.*, 2005, **5**, 1345-1363.
19. H. B. Wang, T. Maiyalagan and X. Wang, *ACS Catal.*, 2012, **2**, 781-794.
20. Q. H. Yang, W. H. Xu, A. Tomita and T. Kyotani, *Chem. Mater.*, 2005, **17**, 2940-2945.
21. J. Wei, D. Zhou, Z. Sun, Y. Deng, Y. Xia and D. Zhao, *Adv. Funct. Mater.*, 2013, **23**, 2322-2328.
22. L.-F. Chen, X.-D. Zhang, H.-W. Liang, M. Kong, Q.-F. Guan, P. Chen, Z.-Y. Wu and S.-H. Yu, *ACS Nano*, 2012, **6**, 7092-7102.
23. X. Meng, H. Cui, J. Dong, J. Zheng, Y. Zhu, Z. Wang, J. Zhang, S. Jia, J. Zhao and Z. Zhu, *J. Mater. Chem. A*, 2013, **1**, 9469-9476.
24. Z. Lei, M. Zhao, L. Dang, L. An, M. Lu, A.-Y. Lo, N. Yu and S.-B. Liu, *J. Mater. Chem.*, 2009, **19**, 5985-5995.
25. A. Sánchez-Sánchez, F. Suárez-García, A. Martínez-Alonso and J. M. Tascón, *Carbon*, 2014, **70**, 119-129.
26. T. Horikawa, N. Sakao, T. Sekida, J. i. Hayashi, D. Do and M. Katoh, *Carbon*, 2012, **50**, 1833-1842.
27. Y. Zheng, Y. Jiao, M. Jaroniec, Y. G. Jin and S. Z. Qiao, *Small*, 2012, **8**, 3550-3566.
28. Y. Liang, H. Liu, Z. Li, R. Fu and D. Wu, *J. Mater. Chem. A*, 2013, **1**, 15207-15211.
29. S. Zhang, A. Ikoma, K. Ueno, Z. Chen, K. Dokko and M. Watanabe, *ChemSusChem*, 2015, **8**, 1608-1617.
30. M. Nandi, K. Okada, A. Dutta, A. Bhaumik, J. Maruyama, D. Derks and H. Uyama, *Chem. Commun.*, 2012, **48**, 10283-10285.
31. M. Zhong, S. Natesakhawat, J. P. Baltrus, D. Luebke, H. Nulwala, K. Matyjaszewski and T. Kowalewski, *Chem. Commun.*, 2012, **48**, 11516-11518.
32. S. Zhang, T. Mandai, K. Ueno, K. Dokko and M. Watanabe, *Nano Energy*, 2015, **13**, 376-386.
33. J. Wang, I. Senkowska, M. Oschatz, M. R. Lohe, L. Borchardt, A. Heerwig, Q. Liu and S. Kaskel, *J. Mater. Chem. A*, 2013, **1**, 10951-10961.
34. M. Zhou, F. Pu, Z. Wang and S. Guan, *Carbon*, 2014, **68**, 185-194.
35. S. Gao, Y. Chen, H. Fan, X. Wei, C. Hu, H. Luo and L. Qu, *J. Mater. Chem. A*, 2014, **2**, 3317-3324.
36. J. Wang, I. Senkowska, M. Oschatz, M. R. Lohe, L. Borchardt, A. Heerwig, Q. Liu and S. Kaskel, *ACS Appl. Mater. Inter.*, 2013, **5**, 3160-3167.
37. X. Zhao, H. Zhao, T. Zhang, X. Yan, Y. Yuan, H. Zhang, H. Zhao, D. Zhang, G. Zhu and X. Yao, *J. Mater. Chem. A*, 2014, **2**, 11666-11671.
38. J.-M. Gu, W.-S. Kim, Y.-K. Hwang and S. Huh, *Carbon*, 2013, **56**, 208-217.
39. M. Zhong, E. K. Kim, J. P. McGann, S. E. Chun, J. F. Whitacre, M. Jaroniec, K. Matyjaszewski and T. Kowalewski, *J. Am. Chem. Soc.*, 2012, **134**, 14846-14857.
40. P. Kuhn, A. Forget, D. S. Su, A. Thomas and M. Antonietti, *J. Am. Chem. Soc.*, 2008, **130**, 13333-13337.
41. D. Puthusseri, V. Aravindan, S. Madhavi and S. Ogale, *Energy Environ. Sci.*, 2014, **7**, 728-735.
42. J. S. Lee, X. Q. Wang, H. M. Luo, G. A. Baker and S. Dai, *J. Am. Chem. Soc.*, 2009, **131**, 4596-4597.
43. M. Zhong, E. K. Kim, J. P. McGann, S.-E. Chun, J. F. Whitacre, M. Jaroniec, K. Matyjaszewski and T. Kowalewski, *J. Am. Chem. Soc.*, 2012, **134**, 14846-14857.
44. S. E. Skrabalak and K. S. Suslick, *J. Am. Chem. Soc.*, 2006, **128**, 12642-12643.
45. D. Hines, A. Bagreev and T. J. Bandosz, *Langmuir*, 2004, **20**, 3388-3397.
46. B. Xu, H. Duan, M. Chu, G. Cao and Y. Yang, *J. Mater. Chem. A*, 2013, **1**, 4565-4570.

- 47.K. Kamegawa, M. Kodama, K. Nishikubo, H. Yamada, Y. Adachi and H. Yoshida, *Microporous Mesoporous Mater.*, 2005, **87**, 118-123.
- 48.C. Knöfel, J. Descarpentries, A. Benzaouia, V. Zelenák, S. Mornet, P. Llewellyn and V. Hornebecq, *Microporous Mesoporous Mater.*, 2007, **99**, 79-85.
- 49.A. Demessence, D. M. D'Alessandro, M. L. Foo and J. R. Long, *J. Am. Chem. Soc.*, 2009, **131**, 8784-8786.
- 50.R. Dawson, D. J. Adams and A. I. Cooper, *Chemical Science*, 2011, **2**, 1173-1177.
- 51.S. Himeno, T. Komatsu and S. Fujita, *J. Chem. Eng. Data*, 2005, **50**, 369-376.
- 52.G. P. Hao, W. C. Li, D. Qian and A. H. Lu, *Adv. Mater.*, 2010, **22**, 853-857.
- 53.S. Zhang, K. Dokko and M. Watanabe, *Chem. Mater.*, 2014, **26**, 2915-2926.
- 54.G. P. Hao, W. C. Li, D. Qian, G. H. Wang, W. P. Zhang, T. Zhang, A. Q. Wang, F. Schuth, H. J. Bongard and A. H. Lu, *J. Am. Chem. Soc.*, 2011, **133**, 11378-11388.
- 55.M. Sevilla, P. Valle-Vigón and A. B. Fuertes, *Adv. Funct. Mater.*, 2011, **21**, 2781-2787.
- 56.V. Chandra, S. U. Yu, S. H. Kim, Y. S. Yoon, D. Y. Kim, A. H. Kwon, M. Meyyappan and K. S. Kim, *Chem. Commun.*, 2012, **48**, 735-737.
- 57.M. Nandi, K. Okada, A. Dutta, A. Bhaumik, J. Maruyama, D. Derks and H. Uyama, *Chem. Commun.*, 2012, **48**, 10283-10285.
- 58.K. S. W. Sing, D. H. Everett, R. A. W. Haul, L. Moscou, R. A. Pierotti, J. Rouquerol and T. Siemieniowska, *Pure Appl. Chem.*, 1985, **57**, 603-619.
- 59.S. C. Moldoveanu, ed. 2010.
- 60.S. Maldonado, S. Morin and K. J. Stevenson, *Carbon*, 2006, **44**, 1429-1437.
- 61.K. Fahsi, S. G. Dutremez, A. Vioux and L. Viau, *J. Mater. Chem. A*, 2013, **1**, 4451-4461.
- 62.X. Ning, W. Zhong, S. Li, Y. Wang and W. Yang, *J. Mater. Chem. A*, 2014, **2**, 8859-8867.
- 63.A. C. Ferrari and J. Robertson, *Phys. Rev. B*, 2000, **61**, 14095-14107.
- 64.S. Reich and C. Thomsen, *Philosophical Transactions of the Royal Society a-Mathematical Physical and Engineering Sciences*, 2004, **362**, 2271-2288.
- 65.K. Ghosh, M. Kumar, T. Maruyama and Y. Ando, *Carbon*, 2010, **48**, 191-200.
- 66.Y. J. Cho, H. S. Kim, S. Y. Baik, Y. Myung, C. S. Jung, C. H. Kim, J. Park and H. S. Kang, *J. Phys. Chem. C*, 2011, **115**, 3737-3744.
- 67.A. Cuesta, P. Dhamelincourt, J. Laureyns, A. Martinezalonso and J. M. D. Tascon, *Carbon*, 1994, **32**, 1523-1532.
- 68.K. Fujisawa, T. Tojo, H. Muramatsu, A. L. Elias, S. M. Vega-Diaz, F. Tristan-Lopez, J. H. Kim, T. Hayashi, Y. A. Kim, M. Endo and M. Terrones, *Nanoscale*, 2011, **3**, 4359-4364.
- 69.F. McFeely, S. Kowalczyk, L. Ley, R. Cavell, R. Pollak and D. Shirley, *Phys. Rev. B*, 1974, **9**, 5268.
- 70.K. R. Lovelock, I. J. Villar-Garcia, F. Maier, H.-P. Steinrück and P. Licence, *Chem. Rev.*, 2010, **110**, 5158-5190.
- 71.T. Sharifi, G. Hu, X. E. Jia and T. Wagberg, *ACS Nano*, 2012, **6**, 8904-8912.
- 72.S. Zhang, S. Tsuzuki, K. Ueno, K. Dokko and M. Watanabe, *Angew. Chem. Int. Ed.*, 2015, **54**, 1302-1306.
- 73.J. Pels, F. Kapteijn, J. Moulijn, Q. Zhu and K. Thomas, *Carbon*, 1995, **33**, 1641-1653.
- 74.S. Chen, J. Bi, Y. Zhao, L. Yang, C. Zhang, Y. Ma, Q. Wu, X. Wang and Z. Hu, *Adv. Mater.*, 2012, **24**, 5593-5597.
- 75.C. H. Choi, S. H. Park and S. I. Woo, *Green Chem.*, 2011, **13**, 406-412.
- 76.S. M. Mahurin, P. F. Fulvio, P. C. Hillesheim, K. M. Nelson, G. M. Veith and S. Dai, *ChemSusChem*, 2014, **7**, 3284-3289.
- 77.A. Vishnyakov, P. I. Ravikovitch and A. V. Neimark, *Langmuir*, 1999, **15**, 8736-8742.
- 78.J. M. Martinmartinez, R. Torregrosamacia and M. C. Mittelmeijerhazeleger, *Fuel*, 1995, **74**, 111-114.
- 79.D. CazorlaAmoros, J. AlcanizMonge and A. LinaresSolano, *Langmuir*, 1996, **12**, 2820-2824.
- 80.X. Zhu, C. Tian, S. Chai, K. Nelson, K. S. Han, E. W. Hagaman, G. M. Veith, S. M. Mahurin, H. Liu and S. Dai, *Adv. Mater.*, 2013, **25**, 4152-4158.
- 81.S. Feng, W. Li, Q. Shi, Y. Li, J. Chen, Y. Ling, A. M. Asiri and D. Zhao, *Chem. Commun.*, 2014, **50**, 329-331.
- 82.L. Wang and R. T. Yang, *J. Phys. Chem. C*, 2011, **115**, 21264-21272.
- 83.Y. Gogotsi, C. Portet, S. Osswald, J. M. Simmons, T. Yildirim, G. Laudisio and J. E. Fischer, *Int. J. Hydrogen Energy*, 2009, **34**, 6314-6319.
- 84.B. B. Saha, S. Jribi, S. Koyama and I. I. El-Sharkawy, *Journal of Chemical & Engineering Data*, 2011, **56**, 1974-1981.
- 85.Y. Xia, R. Mokaya, G. S. Walker and Y. Zhu, *Adv. Energy Mater.*, 2011, **1**, 678-683.
- 86.H. Seema, K. C. Kemp, N. H. Le, S.-W. Park, V. Chandra, J. W. Lee and K. S. Kim, *Carbon*, 2014, **66**, 320-326.
- 87.Y. Xia, Y. Zhu and Y. Tang, *Carbon*, 2012, **50**, 5543-5553.
- 88.S. Xin, L. Gu, N.-H. Zhao, Y.-X. Yin, L.-J. Zhou, Y.-G. Guo and L.-J. Wan, *J. Am. Chem. Soc.*, 2012, **134**, 18510-18513.

One-step, template-free synthesis of highly porous nitrogen/sulfur-codoped carbons from a single protic salt and their application to CO₂ capture

Shiguo Zhang, Zhe Li, Kazuhide Ueno, Ryoichi Tatara, Kaoru Dokko and Masayoshi Watanabe*



Highly porous N/S-codoped carbons obtained by one-step carbonization of an “all-in-one” protic salt showed great potential for CO₂ capture